Chapter 34
Operation Orbit Options for Asteroid Explorations

Xiaosheng Xin, Lin Liu and Shengxian Yu

Abstract For the exploration of asteroids, especially those with small masses, there are several options for the probe: flybying the asteroid, becoming a satellite of the asteroid, or formation flying with the asteroid. This study focuses on the last two kinds of orbits. For the circulate orbit, the model of the asteroid's gravity field is an important issue. Difficulties will be encountered when constructing the analytical solutions to the circulate orbits. Two kinds of formation flying orbits are considered in this study: (1) around the collinear libration points (CLPs) of the Sun-asteroid system, and (2) directly around the asteroid itself. The asteroid Apophis is used as an example throughout the paper. For the first formation flying strategy, the operation orbits (Lissajous orbits and halo orbits) around the CLP L_1 are firstly constructed in the circular restricted three-body problem (CRTBP), and then generalized to the real force model. For the second formation flying strategy, the operation orbits are firstly constructed using the well-known C-W equation, and then also generalized to the real force model, where the asteroid's true orbit and the solar radiation pressure (SRP) are considered. Studies in this work may be used as references for future asteroid missions.

Keywords Asteroid · Circulate orbit · Formation flying orbit · Libration point · C-W equation

34.1 Introduction

When exploring asteroids, especially those with small masses, one problem is whether the weak gravity field can capture the spacecraft to a satellite orbit around the asteroids. For asteroids with considerable masses, this problem usually does not

X. Xin · L. Liu (✉)
School of Astronomy and Space Science, Nanjing University, Nanjing 210093, China
e-mail: lliu@nju.edu.cn

S. Yu
Purple Mountain Observatory, Chinese Academy of Sciences, Nanjing 210008, China

R. Shen and W. Qian (eds.), *Proceedings of the 27th Conference of Spacecraft TT&C Technology in China*, Lecture Notes in Electrical Engineering 323,
DOI 10.1007/978-3-662-44687-4_34

exist, but another problem is the shape and mass distribution of the asteroids. Generally, asteroids have irregular shapes quite different from the spheres. One example is, the Amor type asteroid, 433 Eros. It has a size of 34.4 × 11.2 × 11.2 km [1]. Another example is the asteroid 25143 Itokawa, which was visited by the Japanese spacecraft Hayabusa launched in May 2003. The asteroid's orthogonal axes are 533, 294 and 209 m [2]. Due to the shape irregularity and possible inhomogeneous mass distribution, the asteroids' gravity fields may be quite different from those of the planets, especially for regions close to the bodies. Many new problems appear, such as modelling of the asteroid gravity field, orbit dynamics (shape, equilibrium points, stability, etc.) in the irregular shaped gravity field with other possible external perturbations (solar and planetary tidal perturbation, SRP). These problems should be considered in designing the orbit, and the guidance, navigation and control (GNC) of the spacecraft, and the ground TT&C operations.

Many works have been done about these problems [3–6]. In this contribution, however, we only briefly discuss the difficulties associated with the construction of analytical solutions to the circulate orbits and then focus on the formation flying orbits. The formation flying orbits are especially suitable and practical for asteroids with weak gravity fields, because usually it is difficult for these asteroids to host a spacecraft as a stable satellite.

Two kinds of formation flying orbits exist. One strategy is that the spacecraft orbit around the asteroid's collinear libration points (L_1 or L_2). In this case the mass of the asteroid is considered and the periodic or quasi-periodic orbits are computed in the Sun-asteroid circular restricted three-body problem (CRTBP). The other strategy is that the spacecraft directly fly around the asteroid itself. The mass of the asteroid is neglected and together with the spacecraft they make formation flying around the Sun. In fact, since the asteroid's mass is extremely small compared with that of the Sun, formation flying orbits around the asteroid itself and around its libration points do not differ much with each other in geometry. For example, according to the data obtained from the Minor Planet Center (MPC) [1] about the Eros gravitational constant $GM = 4.463 \times 10^{-4}$ km^3 s^{-2} and other related orbit parameters, it can be calculated that its libration point L_1/L_2 only deviates about 1,600 km from its center. This distance tends to decrease for asteroids with smaller masses.

These two kinds of formation flying orbits have no fundamental difference. Mathematically, they can be computed with the same method. The only difference lies in whether or not the mass of the asteroid is considered. The formation flying orbits directly around the asteroid neglect the asteroid's mass while the formation flying orbits around the collinear libration points consider it. We still treat them as distinct cases in this paper for clarity.

34.2 Difficulties of Constructing Analytical Solutions to Circulate Orbits

The circulate orbits for proximity exploration of asteroids are mainly affected by the non-spherical and third-body (the Sun and major planets) gravitation. The treatment of the latter force is relatively easy. But problems would be encountered when computing the former one. The first problem is the modelling of the gravity field. We will not elaborate on the different methods here but examine the main physical parameters of the gravity field of an example asteroid 433 Eros [1], which are shown in Tables 34.1 and 34.2.

For comparison, the gravitational constants of the Sun and the Earth are listed as follows:

$$GS = 1.32712442076 \times 10^{11}\,\mathrm{km^3\,s^{-2}}, \quad GE = .986004418 \times 10^{5}\,\mathrm{km^3\,s^{-2}}$$

Table 34.1 The gravity field model for asteroid 433 Eros ($R_0 = 16.0$ km)

l, m	$\overline{C}_{l,m}$	$\overline{S}_{l,m}$
2, 0	−0.052478	0
2, 1	0	0
2, 2	0.082538	−0.027745
3, 0	−0.001400	0
3, 1	0.004055	0.003379
3, 2	0.001792	−0.000686
3, 3	−0.010337	−0.012134
4, 0	0.012900	0
4, 1	−0.000106	0.000136
4, 2	−0.017495	0.004542
4, 3	−0.000319	−0.000141
4, 4	0.017587	−0.008939

Table 34.2 Main physical parameters of asteroid 433 Eros

Parameters	Values
Volume	$2503 \pm 25\,\mathrm{km^3}$
Bulk density	$2.67 \pm 0.03\,\mathrm{g\,cm^{-3}}$
Mass	$(6.6904 \pm 0.0030) \times 10^{15}$ kg
GM (optical radiometric)	$(4.4631 \pm 0.0003) \times 10^{-4}\,\mathrm{km^3\,s^{-2}}$
GM (radiometric)	$(4.4584 \pm 0.0030) \times 10^{-4}\,\mathrm{km^3\,s^{-2}}$
GM (radiometric and optical pole)	$(4.4621 \pm 0.0015) \times 10^{-4}\,\mathrm{km^3\,s^{-2}}$
Rotation rate	$1639.38922 \pm 0.00020\,^\circ/\mathrm{day}$

From the values of the main terms of the gravity field $C_{2,0}$ and $C_{2,2}$, it is apparent that the characteristics like that of the Earth gravity field no longer exists. Though difficulties can be overcome to construct the perturbation solutions under certain circumstances, the large values of the oblateness $(C_{2,0})$ and equatorial ellipticity ($C_{2,2}$ and $S_{2,2}$) would cause trouble when determining the number of terms needed for the small parameter power series solutions. In addition, the nonautonomous tesseral terms $C_{2,2}$ and $S_{2,2}$ also pose great challenges for the construction of the analytical orbit solutions. In the worst case, when the orbit eccentricity of the spacecraft is too large, they would cause the construction process to fail [7].

The above discussion is based on the assumption that the asteroid's gravity field can still be modeled with spherical harmonics. For those asteroids with extremely irregular shape and mass distribution that spherical harmonics are almost impossible to approximate, other approaches are needed.

34.3 Formation Flying Orbit Option—Orbit Around the Libration Points

For the formation flying of two earth satellites in close proximity, both their masses can be neglected which is the basic theoretical priority of solving this problem. However, when both satellites are heavy enough, such as those large GEO satellites (several tons) positioned in the 'same' location (about 100 m apart) above the earth equator, obtaining their precise orbits entail the careful consideration of their mutual gravitation [8]. This can be solved from two different approaches. One method is to add their mutual attraction as one additional perturbation force in their respective force model. The other is a whole new mathematical treatment that involves the model of the CRTBP, which we elaborate in the following.

For asteroids with small masses, such as Eros, orbits around its libration point L_1/L_2, which is close to its center, can serve the purpose of formation flying around the asteroid.

34.3.1 Nominal Orbits Around the Libration Points

In this section, we take the L_1 libration point as an example. We adopt the multiple shooting method to construct its Lissajous and halo orbits in the real force model. The high-order analytical solutions of the Lissajous and halo orbits are taken as initial values for the iteration process. The real force model is based on the Sun-Earth-asteroid CRTBP with additional perturbations by the eight major planets as well as Pluto and the Moon.

34.3.1.1 High-Order Solutions of the Lissajous and Halo Orbits

In the synodic coordinate system where the origin coincides with the barycentre of the two primaries, the equation of motion of the CRTBP [9] is

$$\begin{cases} \ddot{X} - 2\dot{Y} = \Omega_X \\ \ddot{Y} + 2\dot{X} = \Omega_Y \\ \ddot{Z} + Z = \Omega_Z \end{cases} \tag{34.1}$$

$$\Omega = \frac{1}{2}\left(X^2 + Y^2\right) + (1-\mu)r_1^{-1} + \mu r_2^{-1}, \quad \begin{cases} r_1^2 = (X-\mu)^2 + Y^2 + Z^2 \\ r_2^2 = (X-\mu+1)^2 + Y^2 + Z^2 \end{cases} \tag{34.2}$$

where $\mu = M/(S+M)$ is the non-dimensional mass of the asteroid.

We change the origin from the barycentre to the L_1 point and magnify the size of the coordinate by a factor of $1/\gamma$, then

$$x = -\frac{1}{\gamma}(X - \mu + 1 - \gamma), \quad y = -\frac{1}{\gamma}Y, \quad z = \frac{1}{\gamma}Z \tag{34.3}$$

in which γ is the distance between the libration point L_1 and the asteroid. In the new coordinate system, the equation of motion becomes

$$\begin{aligned} \ddot{x} - 2\dot{y} - (1+2c_2)x &= \frac{\partial}{\partial x}\sum_{n\geq 3} c_n r^n P_n\left(\frac{x}{r}\right) \\ \ddot{y} + 2\dot{x} + (c_2 - 1)y &= \frac{\partial}{\partial y}\sum_{n\geq 3} c_n r^n P_n\left(\frac{x}{r}\right) \\ \ddot{z} + c_2 z &= \frac{\partial}{\partial z}\sum_{n\geq 3} c_n r^n P_n\left(\frac{x}{r}\right) \end{aligned} \tag{34.4}$$

where P_n is the Legendre polynomials, $r^2 = x^2 + y^2 + z^2$, and the coefficients of the expansion is given by

$$c_n = \gamma^{-3}\left[\mu + (-1)^n(1-\mu)\left(\frac{\gamma}{1-\gamma}\right)^{n+1}\right] \tag{34.5}$$

The solution of Eq. (34.4) yields the Lissajous orbit around the L_1 libration point, which is represented by the following trigonometric series:

$$\begin{cases} x(t) = \sum\limits_{i,j=1}^{\infty} \left(\sum\limits_{|k|\le i,|m|\le j} x_{ijkm} \cos(k\theta_1 + m\theta_2) \right) \alpha^i \beta^j \\ y(t) = \sum\limits_{i,j=1}^{\infty} \left(\sum\limits_{|k|\le i,|m|\le j} y_{ijkm} \sin(k\theta_1 + m\theta_2) \right) \alpha^i \beta^j \\ z(t) = \sum\limits_{i,j=1}^{\infty} \left(\sum\limits_{|k|\le i,|m|\le j} z_{ijkm} \cos(k\theta_1 + m\theta_2) \right) \alpha^i \beta^j \end{cases} \tag{34.6}$$

where $\theta_1 = \omega t + \phi_1$, $\theta_2 = vt + \phi_2$, ϕ_1, ϕ_2 are constants, $N = i + j$ is the order of the solution. In the summation symbol, $i, j = 1$ signifies $i + j = 1, i \ge 0, j \ge 0$. ω, v can be represented by the series in the form

$$\omega = \sum_{i,j=0}^{\infty} \omega_{ij} \alpha^i \beta^j, \quad v = \sum_{i,j=0}^{\infty} v_{ij} \alpha^i \beta^j \tag{34.7}$$

The higher-order solution can be derived from the lower-order solution. Therefore, the solution obtained from the linearized model can serve as the initial value for the recurrence.

Normally, ω and v are not commensurate with each other. But when the amplitude of in-plane α and out-of-plane β are large enough, some of the combinations of the two amplitudes would yield $\omega = v$. This is the case of periodic orbit in the 3D space, which is also named as halo orbit. The halo orbit can be represented as expansion of the trigonometric series in the form:

$$\begin{cases} x(t) = \sum\limits_{i,j=1}^{\infty} \left(\sum\limits_{|k|\le i} x_{ijk} \cos(k\theta) \right) \alpha^i \beta^j \\ y(t) = \sum\limits_{i,j=1}^{\infty} \left(\sum\limits_{|k|\le i} y_{ijk} \sin(k\theta) \right) \alpha^i \beta^j \\ z(t) = \sum\limits_{i,j=1}^{\infty} \left(\sum\limits_{|k|\le i} z_{ijk} \cos(k\theta) \right) \alpha^i \beta^j \end{cases} \tag{34.8}$$

The detailed derivation already exists in the literature [10–12].

We take asteroid Apophis as an example. On JD = 2455800.5, its orbital elements are

$$\begin{cases} a = 0.9223002432\ AU, & e = 0.1910762290, & i = 3.3319600435^\circ \\ \Omega = 204.4304100445^\circ, & \omega = 126.4244766663^\circ, & M = 287.5823055950^\circ \end{cases},$$

and its mass is $M_a = 2.7 \times 10^{10}$ kg. The non-dimensional units are taken as

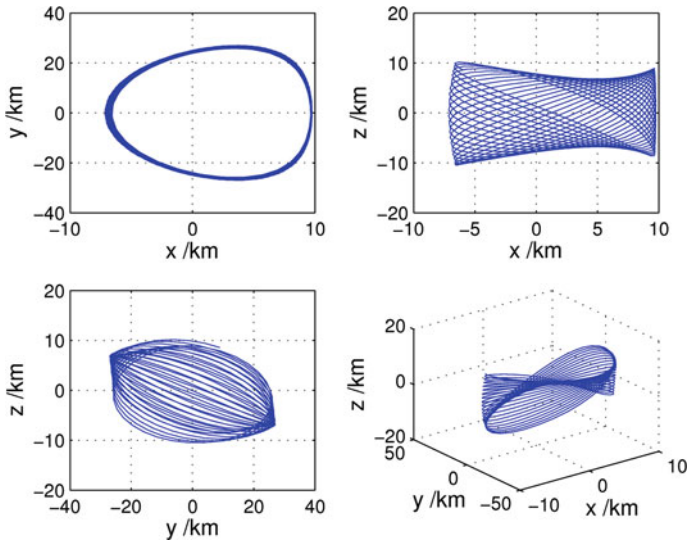

Fig. 34.1 Lissajous orbits around the Apophis L_1 libration point ($\alpha = \beta = 2 \times 10^{-8} R_0$)

$$\begin{cases} [L] = R_0 = 0.9223002432 \text{ AU}, \\ [M] = M_{\text{sun}} + M_{\text{a}}, \\ [T] = \left[R_0^3 / G(M_{\text{sun}} + M_{\text{a}})\right]^{1/2} \approx 51.490492199842 \text{ d} \end{cases} \tag{34.9}$$

Without special notice, all quantities below are expressed in the non-dimensional units. The orbit insertion time is 00:00:00 March 14, 2018, which corresponds to Julian Date JD = 2458191.5. The orbits around the L_1 point are shown here as an example. The Lissajous and halo orbits are shown in Figs. 34.1 and 34.2, respectively, where $\gamma = 1.653975024 \times 10^{-7}$.

34.3.1.2 Numerical Computation of the Lissajous and Halo Orbits in Real Force Model

Taking the third-order analytical solutions as initial values, we find the Lissajous and halo orbits in the real force model via multiple shooting method (i.e. differential correction). The real force model is based on the Sun-Earth-asteroid CRTBP with additional perturbations by the eight major planets as well as Pluto and the Moon, whose ephemerides are given by DE 405. The ephemeris of the asteroid is obtained by integration in this real force model. The Lissajous and halo orbits computed are depicted in Figs. 34.3 and 34.4, respectively.

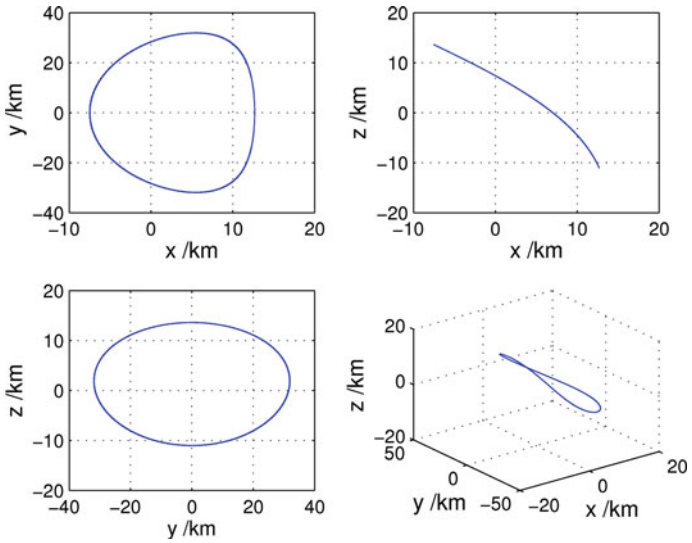

Fig. 34.2 Halo orbits around the Apophis L_1 libration point ($\alpha = 2.48 \times 10^{-8} R_0$)

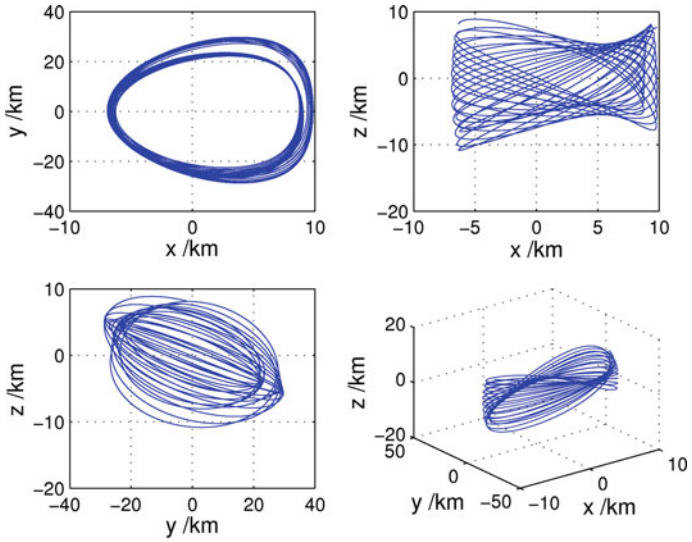

Fig. 34.3 Lissajous orbits around the Apophis L_1 libration point in the real force model ($\alpha = \beta = 2 \times 10^{-8} R_0$)

Comparing the orbits obtained by the third-order analytical solutions and those computed in the real force model, we can find that the two kinds of orbits, especially the halo orbits, have larger drifting regions in the real force model scenario

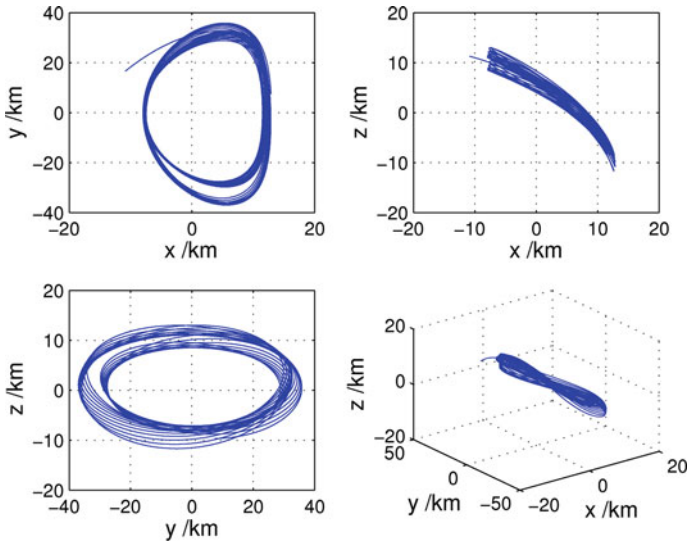

Fig. 34.4 Halo orbits around the Apophis L_1 libration point in the real force model ($\alpha = 2.48 \times 10^{-8} R_0$)

due to the perturbations of other celestial bodies. In spite of this, the orbits in the real force model still stay around those produced by the analytical solutions; in other words, they still retain their respective orbit characteristics after certain amount of time.

34.4 Formation Flying Orbit Option—Orbit Around the Asteroid Itself

If the asteroid's mass is so small that it can be neglected, i.e. the mass parameter $\mu = M/(S+M) = 0$, then the above case of orbits around the libration points is degenerated to the case of spacecraft formation flying with the asteroid itself. In this case, the L_1 and L_2 libration points merge together with the center of the asteroid $(x = 1, y = 0, z = 0)$, and the corresponding equation of motion can be obtained from Eq. (34.4) with $c_2 = 1$ [13]. The linearized form is just the C-W equation [14] well-known in the satellite formation flying research. The coordinate symbols are denoted as (ξ, η, ζ) instead of (x, y, z) for discrimination. The linearized equation reads

$$\ddot{\xi} - 2\dot{\eta} = 3\xi, \quad \ddot{\eta} + 2\dot{\xi} = 0, \quad \ddot{\varsigma} + \varsigma = 0 \tag{34.10}$$

34.4.1 Solutions of Conditional Periodic Orbits in the Linearized Circumstance

The solution of Eq. (34.10) is

$$\begin{cases} \xi = -\dfrac{2}{3}C_2 + \dfrac{1}{2}C_3 \sin t - \dfrac{1}{2}C_4 \cos t \\ \dot{\xi} = \dfrac{1}{2}C_3 \cos t + \dfrac{1}{2}C_4 \sin t \\ \eta = C_1 + C_2 t + C_3 \cos t + C_4 \sin t \\ \dot{\eta} = C_2 - C_3 \sin t + C_4 \cos t \end{cases} \tag{34.11}$$

The motion in the direction of ς is a simple harmonic oscillation. With proper initial values, by setting $C_1 = C_2 = 0$, the conditional periodic solution can be obtained. The initial conditions at time t_0 should satisfy

$$\xi_0,\ \eta_0,\ \dot{\xi}_0 = \eta_0/2,\ \dot{\eta}_0 = -2\xi_0,\ \varsigma_0,\ \dot{\varsigma}_0 \tag{34.12}$$

and the solution is

$$\begin{cases} \xi = \xi_0 \cos t + (\eta_0/2) \sin t, & \dot{\xi} = -\xi_0 \sin t + (\eta_0/2) \cos t \\ \eta = -2\xi_0 \sin t + \eta_0 \cos t, & \dot{\eta} = -2\xi_0 \cos t - \eta_0 \sin t \\ \varsigma = \varsigma_0 \cos t + \dot{\varsigma}_0 \sin t, & \dot{\varsigma} = -\varsigma_0 \sin t + \dot{\varsigma}_0 \cos t \end{cases} \tag{34.13}$$

Its projection on the $\xi-\eta$ plane is an ellipse. In addition, if $\dot{\varsigma}_0$ also satisfies $\dot{\varsigma}_0 = \pm(\eta_0/2\xi_0)\varsigma_0$, the projection on the $\eta-\varsigma$ is also an ellipse. Taking $\xi_0 = \eta_0 = \varsigma_0 = 1 \times 10^{-4} R_0$, we can get the orbit shown in Fig. 34.5. Various formation flying orbits with different configurations can be computed by modifying the initial conditions. The conditional periodic solution (34.13) is later taken as the initial orbit for iteration.

34.4.2 Numerical Result of Formation Flying Around Asteroid Itself in the Real Force Model

In the rotating coordinate system centered on the asteroid, the equation of motion of the spacecraft is

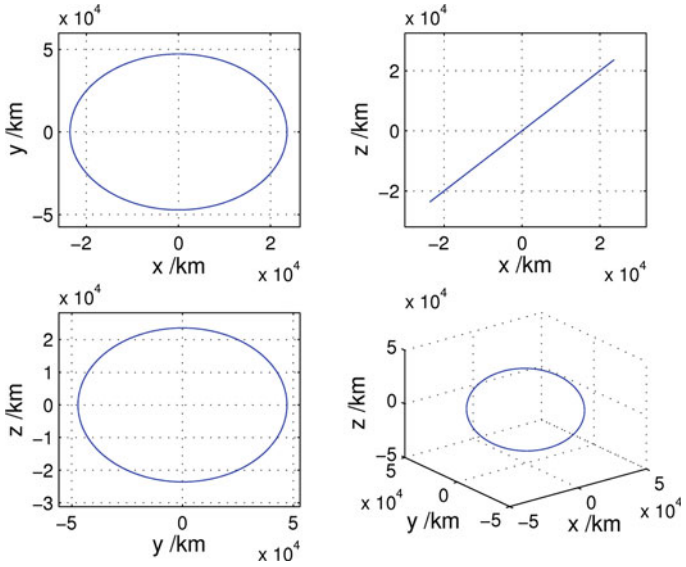

Fig. 34.5 Conditional periodic orbits around Apophis ($\xi_0 = \eta_0 = \varsigma_0 = 1 \times 10^{-4} R_0$)

$$
\begin{aligned}
&\ddot{\boldsymbol{\rho}} = \mathbf{F}_1 + \mathbf{F}_2 \\
&\mathbf{F}_1 = -2C^T\dot{C}\dot{\boldsymbol{\rho}} - C^T\ddot{C}\boldsymbol{\rho} - \mu_{11}\mathbf{r}/r^3 + \mu_{11}\mathbf{r}_{12}/r_{12}^3 - \sum_{i\in S, i\neq 11,12}\mu_i\left(\boldsymbol{\delta}_i/\delta_i^3 - \boldsymbol{\delta}_i^{12}/\left(\delta_i^{12}\right)^3\right) \\
&\mathbf{F}_2 = -\mu_{11}\mathbf{r}_{12}/r_{12}^3 - \sum_{i\in S, i\neq 11,12}\mu_i\left(\boldsymbol{\delta}_i^{12}/\left(\delta_i^{12}\right)^3 + \mathbf{r}_i/r_i^3\right) - \ddot{\mathbf{r}}_{12} - 2C^T\dot{C}\dot{\mathbf{r}}_{12} - C^T\ddot{C}\mathbf{r}_{12}
\end{aligned}
\tag{34.14}
$$

where $\mathbf{r}, \mathbf{r}_i$ is the position vector in the Sun-centered rotating system, $\mathbf{r}$ is the position vector of the spacecraft, and $\mathbf{r}_i$ is the position vector of the major planet μ_i. $\boldsymbol{\rho}(\xi, \eta, \zeta) = \mathbf{r} - \mathbf{r}_{12}$ is the position vector of the spacecraft relative to the asteroid, and $\boldsymbol{\delta}_{12}^i = \mathbf{r}_{12} - \mathbf{r}_i$ is the position vector of the asteroid relative to the major planet μ_i. C is the transformation matrix between the Sun-centered rotating system and the Sun-centered inertial coordinate system.

Using the orbit obtained in Sect. 34.4.1 as initial value, we have computed the corrected conditional quasi-periodic orbit in the real force model via multiple shooting method, which is shown in Fig. 34.6.

Figure 34.6 shows the change of the orbit over 8.458 years. It can be seen that although perturbations of major planets and orbit evolution of the asteroid are considered in the real force model the corrected orbit still stays in the vicinity of the orbit calculated from the solution of linearized model, only with minor drift relative to the initial orbit.

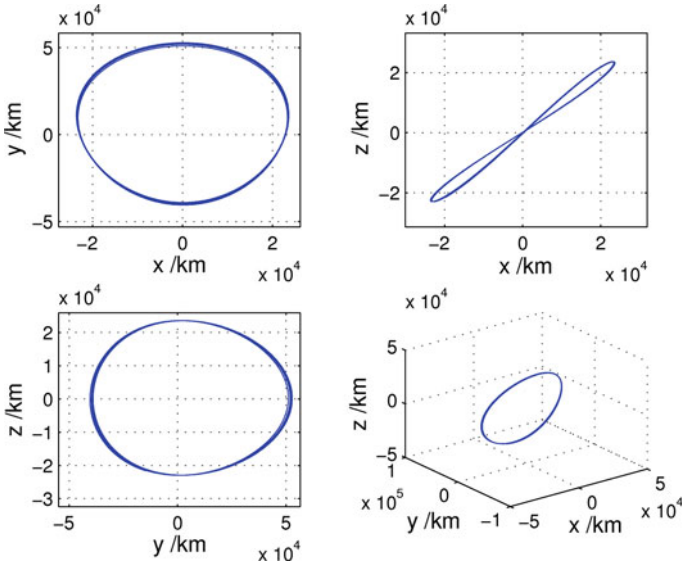

Fig. 34.6 Conditional quasi-periodic orbits around Apophis in the real force model ($\xi_0 = \eta_0 = \varsigma_0 = 1 \times 10^{-4} R_0$)

The above computation does not take into account the gravity effect of the asteroid on the spacecraft. Taking this factor into consideration as a perturbation, with the same initial orbit for ephemeris integration, the difference between the resultant 'true' orbit and the nominal orbit in Fig. 34.6 is shown in Fig. 34.7.

Figure 34.7 tells us that the effect of neglecting Apophis' mass on the orbit with altitude of $O(10^4)$ km over 8.458 years is on the order of $O(10^2)$ m. Therefore, the nominal orbit is not influenced much without considering the asteroid's mass.

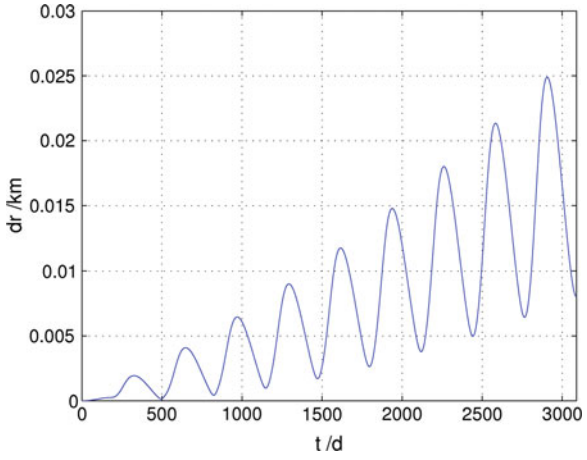

Fig. 34.7 Difference between the 'true' orbit considering the Apophis mass and the nominal orbit

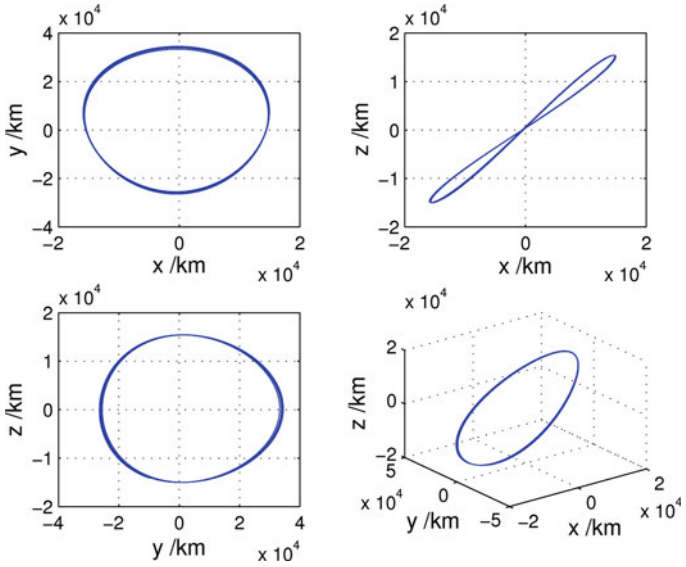

Fig. 34.8 Conditional periodic orbit around Apophis in the real force model with SRP perturbation. ($\xi_0 = \eta_0 = \varsigma_0 = 1 \times 10^{-4} R_0$)

34.4.3 Effect of the SRP Perturbation on Formation Flying Orbit

The origin of the formation flying orbit is still the asteroid's center after taking the perturbation of SRP into account. As a result, the orbit calculated from the analytical solution is the same as in Fig. 34.6. For the real force model, the perturbation of SRP should be added to the model to numerically correct the initial orbit. The final orbit is shown in Fig. 34.8.

34.5 Conclusion

In this paper, we proposed two kinds of orbits for asteroid explorations, the formation flying orbits around the collinear libration points of the asteroid and the formation flying orbits around the asteroid itself. Which kind of orbits should be used depends on the mass of the asteroid. Moreover, under certain circumstances, the SRP perturbation should also be considered, but no differences appear in the numerical method described in the paper.

Orbit control to the two kinds of formation flying orbits is necessary, because both of them are unstable. We also did some work on this topic, with two possible approaches: continuous low-thrust and solar sail. We leave this topic for future discussions.

References

1. Miller JK et al (2002) Determination of shape, gravity, and rotational state of asteroid 433 Eros. Icarus 155(1):3–17
2. Saito J et al (2006) Detailed images of asteroid 25143 Itokawa from Hayabusa. Science 312 (5778):1341–1344
3. Werner RA, Scheeres DJ. Exterior gravitation of a polyhedron derived and compared with harmonic and mascon gravitation representations of asteroid 4769 Castalia. Celestial Mech Dyn Astron 65(3):313–344
4. Scheeres DJ (1994) Dynamics about uniformly rotating triaxial ellipsoids: applications to asteroids. Icarus 110(2):225–238
5. Scheeres DJ et al (1996) Orbits close to asteroid 4769 Castalia. Icarus 121(1):67–87
6. Scheeres DJ et al (1996) Dynamics of orbits close to asteroid 4179 Toutatis. Icarus 132 (1):53–79
7. Liu L (2000) Orbit theory of spacecraft. Defense industry press, Beijing
8. Zhang Q, Liu L (1999) On the binary star system of geostationary satellites. J Nanjing Univ 35:7–13
9. Liu L, Hou XY (2012) Deep space spacecraft orbit dynamics. Publishing House of Electronics Industry, Beijing
10. Jorba A, Masdemont J (1999) Dynamics in the center manifold of the collinear points of the restricted three body problem. Phys D: Nonlinear Phenom 132(1):189–213
11. Richardson DL (1980) Analytic construction of periodic orbits about the collinear points. Celest Mech 22(3):241–253
12. Kim M (2001) Periodic spacecraft orbits for future space-based deep space observations. Technical report, Vienna Institute of Technology, Vienna
13. Liu L, Wang HH, Ma JB (2004) On the formation flying of satellite constellations. Chin Astron Astrophys 28(2):188–199
14. Clohessy WH (1960) Terminal guidance system for satellite rendezvous. J Aerosp Sci 27:653–658